A Thermo-Hydraulic Numerical Model for High Energy Welding Processes

Marc Medale* — Sylvain Rabier* — Charline Xhaard*,**

** Polytech' Marseille, Lab. de l'IUSTI, UMR 6595 CNRS - Université de Provence*
Technopole de Château-Gombert, 5 rue Enrico Fermi
13453 Marseille Cedex 13

*** CEA, Centre de Valduc, DAM/DFTN*
21120 IS sur TILLE

Marc.Medale@polytech.univ-mrs.fr

ABSTRACT. *A numerical model especially devoted to the thermal simulation of high energy welding processes is proposed in this paper. It suggests one possible way to overcome the difficulty to simultaneously deal in the same numerical model with solid, liquid, and gas phases, together with their intense interactions. The proposed model results in a rather simplified model in the gas phase associated with a much more detailed one in the condensed phase (solid, liquid and mushy). The resulting numerical model is based on the finite element method, and features the dynamical evolution of the gas-liquid interface (key-hole) together with the liquid-solid one through an enthalpy formulation.*

RÉSUMÉ. *Nous proposons un modèle numérique pour l'étude thermique de procédés de soudage par fusion à haute énergie. Il constitue une voie pour surmonter la principale difficulté, associée à l'existence simultanée des phases solide, liquide et vapeur et de leurs intenses interactions, dans le développement de modèles numériques adaptés à cette classe de problèmes. Le modèle proposé résulte de l'association d'une modélisation simplifiée de la phase gazeuse et d'une modélisation plus approfondie de la phase condensée (solide, liquide, et zone pâteuse). Un modèle numérique basé sur la méthode des éléments finis a été développé pour simuler cette approche thermo-hydraulique du problème. Il considère l'évolution dynamique de l'interface liquide-gaz (key-hole) par un modèle d'écoulement à surface libre, et de l'interface solide-liquide par une formulation enthalpique.*

KEYWORDS: *welding processes modeling, moving interfaces, free surface flows, phase change, incompressible fluid flows, finite element method.*

MOTS-CLÉS : *procédés de soudage, interfaces mobiles, surface libre, changement de phases, thermo-hydraulique, écoulements incompressibles, méthode des éléments finis.*

REEF – 13/2004. Numerical Simulation of Welding, pages 207 to 229

1. Introduction

High energy welding processes (laser beam or electron beam) could be characterized by the simultaneous presence of solid, liquid, and vapour phases together with a very intense interaction between them. Indeed a high vapour discharge induces a strong liquid–gas interface deformation, which results in the keyhole formation. This keyhole significantly interacts with the beam source, which could often lead to defects in the welds. That is the reason why a deep insight is required to prevent from unreliable joints and over-strained assemblies. On the way to better understand the thermo-mechanical evolution of the welded structures, one has to take into account the whole thermal cycle occurring throughout the process. This obviously involves considering the keyhole dynamics, fluid flow in the melt pool and thermo-metallurgical aspects during the cooling stage.

Despite a large amount of research has already been devoted to these aspects, the bibliographical revue brings to light a lack of detailed understanding in some specific fields. Some of these issues discussed in this paper are sketched in figure 1 and will be described in the following. They correspond to the early stages of the whole welding processes associated with high-energy deposition (source-condensed matter interaction, keyhole dynamics -expansion and collapse- together with their related heat transfer and characteristic thermal zones).

First of all, the beam source interaction with the work-piece material depends on several phenomena. For instance, concerning laser beam welding, Fresnel absorption and inverse Bremsstrahlung one govern the interaction. The former indicates that the energy density over the keyhole walls is linked to its shape as it determines the optical path of rays. Moreover, the absorptivity coefficient depends on both the incidence angle (Solana *et al*., 1997) and the local temperature (Duley, 1999). As expected, the high energy density induces a steep temperature elevation, which yields melting and ultimately vaporization of the liquid metal (figure 1a-b). Consequently, the generated intense vapor discharge modifies at its turn the beam source–matter interaction (inverse Bremsstrahlung absorption), which is usually modeled by an attenuation coefficient (in the Beer Lambert law, (Duley, 1999)). In the laser beam case, this coefficient also depends on the ionization degree (one speaks of plume for the lowest ionization levels and plasma for the highest), which could be related to the laser beam wavelength (Ho *et al*., 2003).

Owing to the huge density ratio appearing at the liquid-gas phase change a strong normal stress takes place over the liquid–gas interface: the recoil pressure. One of the first recoil pressure models was established in the limit case of vaporization into vacuum (Anisimov, 1968). This model assumes a thermodynamic equilibrium at the liquid–gas interface that enables to link saturation temperature and pressure.

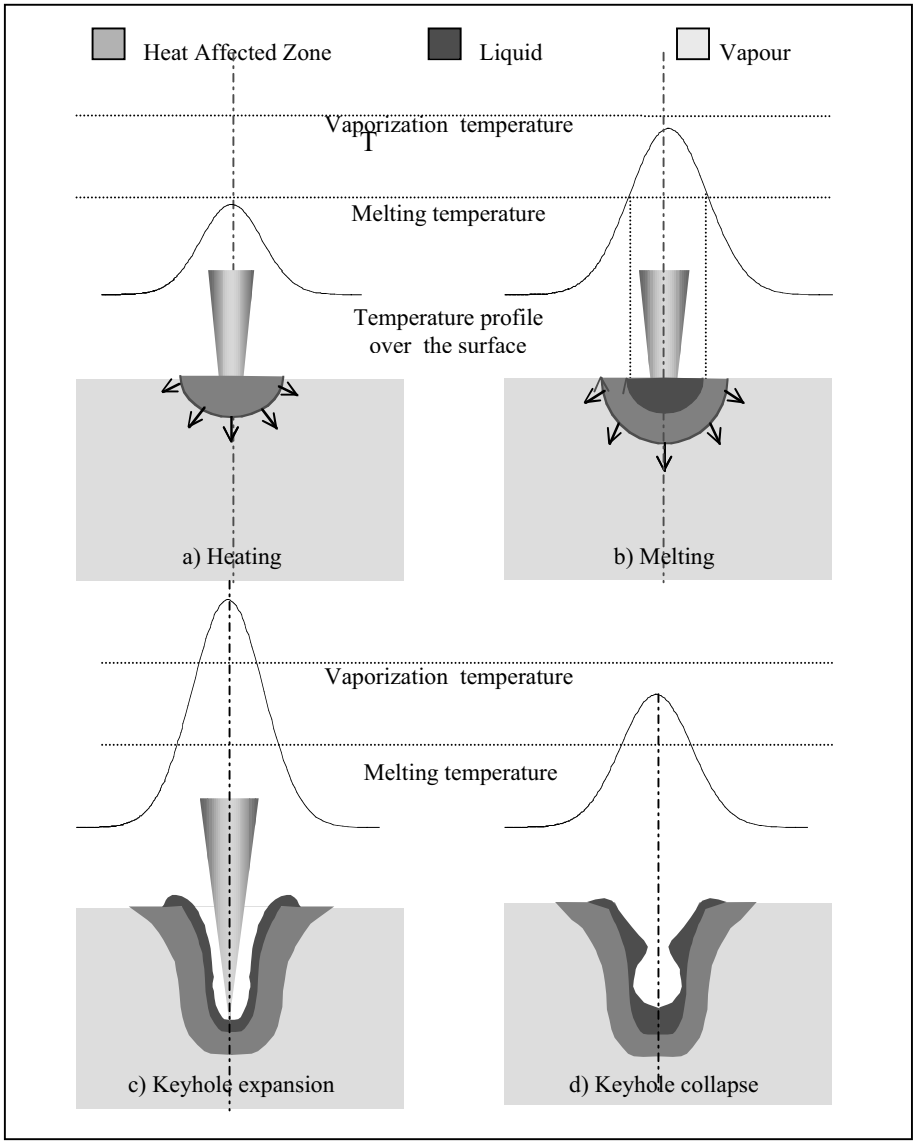

Figure 1. *Sketch of characteristic stages encountered in the keyhole dynamics: a) early heating; b) conductive regime; c) capillary regime; d) collapse and refilling*

A generalization of this approach was later on proposed to take into account the ambient atmosphere influence (Ythreus *et al.*, 1977; Knight, 1979; Knight, 1982)

and was afterward successfully applied to welding and drilling processes (Semak *et al*., 1999). Such a model is of first importance in the high-energy welding processes modeling because the recoil pressure induces a strong liquid–gas interface deformation and a capillary opening forms: the keyhole (figure 1c). So a deeper source penetration compared to the conductive regime is therefore obtained, which in the case of laser beam source is responsible for new kind of interactions. Indeed multiple reflections arise in the keyhole and result in local energy concentrations, inducing thus higher vapor discharge and higher recoil pressure. These phenomena could even produce hydrodynamic instabilities over the keyhole walls (Fabbro *et al*., 2000), and furthermore the higher the velocity gap between the vapor phase and the liquid one is, the more intense are the liquid droplets ejections (Sudnik *et al*., 2000).

The keyhole expansion associated with a high vapor discharge produces significant effects on the whole heat transfer throughout a modified distribution in the energy deposition and the intense advective contribution in the melt (Semak *et al*., 1997). Nevertheless, different levels of hydrodynamic keyhole modeling have been encountered in recent scientific literature. Indeed, for low energy densities yielding a conductive-like regime, the liquid-gas interface deformation could be assumed as negligible and could therefore be omitted in the modeling (He *et al*., 2003). Conversely, for high energy densities when the keyhole plays a significant part in the end weld-joint characteristics, its shape and the related fluid flow in the melted pool can no longer be ignored in any detailed model. Here again, different approaches have been adopted to take into account the keyhole influence on the thermal field. On the one hand, analytical and semi-analytical approaches have allowed to model simplified cases by considering cylindrical symmetry and neglecting non-linear phenomena (phase change enthalpy, radiative heat transfer, variable physical properties, etc.) (Semak *et al*., 1999; Solana *et al*., 1999). On the other hand, numerical models have recently overcome many of these rather restrictive limitations and have enabled a more accurate track of the liquid-gas interface. The solution of incompressible Navier-Stokes equations in both the liquid and gas phases has also been considered (Ganesh *et al*., 1997) in axi-symmetric cases, (Ki *et al*., 2001) in 3D cases. However the approximation of an incompressible vapor flow could be questionable with respect to the actual Mach number (of order of Ma = 0.5) in the phase. When switching off the beam source, the work-piece starts to cool down, the vapor condensation takes progressively place so a fluid flow inversion occurs below the liquid-gas interface and the keyhole finally collapses (figure 1d). During this event, gas bubbles could be captured and converted into pore defects after solidification (Kaplan *et al*., 2002). In order to better predict welds quality both experimental (record of laser pulses by high speed X-Ray imaging) and numerical approaches have been used (Jouvard *et al*., 2001 and Kaplan *et al*., 2002).

The present paper aims to present the finite element model we have developed to compute the heat transfer problem within the condensed phases (solid, mushy and liquid) related to high energy welding processes. The proposed model results in a

simplified model in the gas phase associated with a more detailed one in the condensed phases. It features the dynamical evolution of both the liquid-gas (key-hole) and solid-liquid interfaces thanks to a free surface fluid flow model in the melted pool supplemented with an enthalpy formulation in the whole condensed phases. The paper is organized as follows. The heat transfer governing equations in the condensed phases are recalled in section 2. Next, the developed finite element model is presented in section 3. Then, some model capabilities are outlined in section 4, where results featuring the usual three levels of approximation for the keyhole modeling are discussed. Finally, concluding remarks are given in section 5.

2. Governing equations

In this paper it is our concern to develop a transient macroscopic heat transfer model within the work-piece able to deal with high energy welding processes. This led us in a first stage to emphasize on the condensed phases (solid and liquid) whereas the interactions between the dispersed phases (ambient gas, shield gas and vapors) and the condensed phases enter the model through the boundary conditions at the solid-gas and liquid-gas interfaces. Consequently the two key points of the present model stand on one hand in a simplified modeling of the interaction between the heat source, the dispersed phase and the condensed phases. On the other hand, it features a more comprehensive modeling of the condensed phases taking into account the moving interfaces (both solid-liquid and liquid-vapor) together with the fluid flow in the liquid phase.

As usual the macroscopic model in the condensed phases is derived from the two-phase model (Bennon *et al.*, 1987), (Ni *et al.,* 1995) in which the control volume could contain either purely solid and liquid phases, or a mixture of both phases. Therefore, the conservation equations of mass, momentum and energy apply on the whole condensed matter domain (solid and liquid) with physical properties specific to each phase (Voller *et al.,* 1990). However, in order to deal with alloys, for which the solid-liquid phase change occurs over a temperature range (the mushy zone), we have considered a simplified approach in which the physical properties in the mushy zone result from a weighted average of the solid and liquid ones (Voller *et al.,* 1987). However, since no metallurgical phenomena are considered in the present model, both material properties (solid, mushy and liquid) are in the present model exclusively thermally dependent.

2.1. *Heat transfer model*

At this stage of the model development, the heat source delivery over the work-piece upper surface is modeled in its simplest way through a gaussian distribution:

$$q_{bs} = I_0 \, e^{-\left(r^2 / 2 r_{bs}^2 \right)} \qquad [1]$$

where I_0 is the beam source intensity, r is the distance to the beam axis and r_{bs} is the delivery beam radius. The applied energy density induces first a local melting of the solid metal, so the solid-liquid phase change is taken into account in the present heat transfer model thanks to an enthalpy formulation of the energy conservation equation. This model is quite well suited to deal with non-isothermal solid-liquid phase change problems and besides it leads to a natural numerical model to implement for this class of problems solving. The energy conservation equation in the condensed phases (solid, liquid and mushy) reads in the enthalpy formulation:

$$\rho_i \left[\frac{\partial \left(H + \Delta H \right)}{\partial t} + \left(u . \nabla \right) \left(H + \Delta H \right) \right] = - \nabla . \mathbf{q} + Q_v \qquad [2]$$

where ρ_i designates the i-phase density (i=solid, mushy or liquid), H and ΔH stand for the sensible and latent enthalpies respectively, t the time, **u** the velocity vector (it corresponds to the welding speed in the solid as the reference frame coincides with the beam source, and to the fluid flow velocity in the liquid), **q** is the conductive heat flux and Q_v is a possible internal heat source. Assuming an isotropic thermal conductivity k_i in each i phase (i=solid, mushy or liquid), the Fourier's law reads:

$$\mathbf{q} = - k_i \nabla T \qquad [3]$$

Moreover, the sensible enthalpy is linked to the temperature for solids and incompressible fluids through the specific heat capacity coefficient Cp_i in each i phase (i=solid, mushy or liquid):

$$H = Cp_i \, T \qquad [4]$$

Concerning the latent enthalpy related to the solid-liquid phase change, various phenomenological relationships have been proposed in the literature depending on the physical knowledge of considered alloy (Rappaz, 1989), (Reddy *et al*., 1992). Nevertheless in this paper linear temperature dependence has been adopted:

$$\Delta H = \begin{cases} 0 & \text{if } T < T_{sol} \\ L_{sl} \, f_{liq} & \text{if } T_{sol} \leq T \leq T_{liq} \\ L_{sl} & \text{if } T > T_{liq} \end{cases} \qquad [5]$$

where L_{sl} is the solid-liquid latent heat and f_{liq} stands for the liquid fraction in the mushy zone, which is assumed at its turn to depend linearly on temperature in the solidus-liquidus temperature range:

$$f_{liq} = \frac{T - T_{sol}}{T_{liq} - T_{sol}} \qquad [6]$$

Furthermore, as far as we are concerned with high energy welding processes, liquid metal evaporation should also be considered. The rate of thermal energy devoted to vaporization or condensation is accounted in our model as a boundary condition over the liquid-vapor interface. It is modeled as the product of the rate of vaporization or condensation, times the liquid-vapor latent heat:

$$q_{lv} = \dot{m}_{lv} L_{lv} \qquad [7a]$$

$$\rho_l \mathbf{v}_{l/\Sigma} \cdot \mathbf{n} = \rho_v \mathbf{v}_{v/\Sigma} \cdot \mathbf{n} \qquad [7b]$$

The vaporization rate in [7a] is drawn from the mass balance across the liquid-vapor interface [7b], where $\mathbf{n}$ stands for the unit normal at the liquid-vapor interface Σ.

Finally, radiative and convective heat transfer are also considered over the boundaries of the condensed phase domain, and they are modeled as usual:

$$q_{rc} = \sigma \varepsilon (T^4 - T_\infty^4) + h\left(T - T_\infty\right) \qquad [8]$$

where σ represents the Stefan-Boltzman constant, ε is the surface emissivity, T_∞ designates the far field temperature and h is the convective heat transfer coefficient between the dispersed and the condensed phases.

2.2. *Incompressible fluid flow model*

The heat transfer in the condensed phases could be significantly dominated by advection in the melted pool. Therefore we have modeled the liquid metal dynamics as an incompressible fluid flow. Nevertheless the basic Navier-Stokes equations should be slightly modified in the present case to account at the macroscopic scale for the inter-dendrites fluid flow, which occurs in the mushy zone at the microscopic scale. Therefore, the mass and momentum conservation equations read:

$$\nabla . \mathbf{u} = 0 \qquad [9]$$

$$\rho_l\left[\frac{\partial \mathbf{u}}{\partial t}+\left(\mathbf{u}.\nabla\right)\mathbf{u}\right]=\nabla.\bar{\bar{\sigma}}+\mathbf{f}^{v}+\mathcal{S}^{u} \qquad [10]$$

where $\bar{\bar{\sigma}}$ is the stress tensor, $\mathbf{f}^{v}$ the body force vector and $\mathbf{S}^{u}$ a source term, specific to the mushy zone. The constitutive laws used to close the preceding set of equations read: for Newtonian liquids the stress tensor is related to the thermodynamic pressure (p) and velocity vector (**u**) through the dynamic viscosity coefficient μ:

$$\bar{\bar{\sigma}}=-p\bar{\bar{I}}+\mu\left[\left(\nabla\otimes\mathbf{u}\right)+\left(\nabla\otimes\mathbf{u}\right)^{T}\right] \qquad [11]$$

The Boussinesq approximation is used to take into account buoyancy in the incompressible fluid flow model: the body force is related to the gravity acceleration (**g**) and temperature through the thermal expansion coefficient (β) according to:

$$\mathbf{f}^{v}=\rho_{l_0}\left[1-\beta\left(T-T_0\right)\right]\mathbf{g} \qquad [12]$$

where ρ_{l0} is the liquid metal density evaluated at the reference temperature T_0. On the other hand a source term, which selectively applies only in the mushy zone has been introduced to model at the macroscopic scale the inter-dendrites fluid flow, as a Darcy-like fluid flow in a porous media:

$$\mathcal{S}^{u}=\frac{\mu}{K}\left(\mathbf{u}-\mathbf{u}_{sol}\right) \qquad [13]$$

where K is a permeability coefficient in the mushy zone. It could be related to the liquid fraction through the Kozeny-Karman empirical law:

$$K=K_0\left[\frac{f_{liq}^{3}}{1-f_{liq}^{2}}\right] \qquad [14]$$

where K_0 is a reference permeability coefficient.

The boundary conditions that apply to the liquid metal fluid flow problem read in a formal notation:

$$\mathbf{u}=\mathbf{u}^{\partial\Omega} \quad \text{on } \partial\Omega_{sl} \qquad ; \qquad \mathbf{T}=\bar{\bar{\sigma}}.\mathbf{n}=\mathbf{T}^{\partial\Omega} \quad \text{on } \partial\Omega_{lg} \qquad [15]$$

where $\mathbf{u}^{\partial\Omega}$ is the welding velocity (scan speed) imposed all over the solid-liquid interface $\partial\Omega_{sl}$, whereas $\mathbf{T}^{\partial\Omega}$ is the applied loading vector over the liquid-gas interface $\partial\Omega_{lg}$. The most important interactions between the gas phase and the liquid phase can be attributed to: i) the recoil pressure associated with the evaporation process; ii) the shear stress induced by the high velocity difference between vapor flow (and shield gas) and the liquid metal flow in the key hole; iii) surface tension effects (capillary forces owing to pressure difference across the interface, and thermo-capillary forces over the interface induced by surface tension gradients):

$$\mathbf{T}_l + \mathbf{T}_g + \frac{\gamma}{R}\mathbf{n} + \frac{\partial\gamma}{\partial s}\mathbf{t_g} = 0 \qquad \text{with} \quad \gamma = \gamma_0 + \frac{d\gamma}{dT}\left(T - T_0\right) \qquad [16]$$

where $\mathbf{T}_l$ and $\mathbf{T}_g$ are the stress vectors on each side of the liquid-gas interface (in the liquid and gas phases respectively), γ is its surface tension coefficient (assumed to linearly dependent on temperature), R is the curvature radius of the liquid-gas interface, $\mathbf{n}$ and $\mathbf{t_g}$ are the normal and tangent unit vectors over the interface parameterized with the curvilinear abscissa s.

3. Numerical model

The research code we have developed aims to compute a good estimate of the temperature field in the whole work-piece, which could later on be used if wished as an input to any thermo-metallurgical and/or thermo-mechanical analyses. With respect to this goal and although the thermo-hydraulic problem to be solved consists in the strongly coupled incompressible Navier-Stokes and energy equations, we have used a segregated solution algorithm to build our computational model. This numerical approach allows us to consider separate finite element formulations for the heat transfer problem and the incompressible fluid flow one. As a result, its main advantages stand in a better computer efficiency (reduced size of the algebraic systems and ability to separately select the most efficient solver for each algebraic system to be solved), together with a better ease and flexibility to develop.

3.1. *Segregated algorithm*

Moreover, as far as one is concerned with a moving boundary problem (the liquid-gas interface deforms under the applied thermal loading owing to the liquid metal evaporation and the associated vapor flow, etc.), so specific numerical techniques have to be introduced (Crank, 1988), (Shyy *et al.*, 1996). For that purpose we have chosen to work in a moving mesh framework, which consists at each time step of a necessary transient approach, to update the computational domain (and its associated mesh) to conform the shape of the deforming boundary. As the computational mesh evolves in the course of time, the conservation laws have

been recast into an Arbitrary Lagrangian Eulerian formulation (Hirt *et al*, 1974), (Hughes *et al*, 1981), (Belytschko *et al*, 2000). Therefore the segregated algorithm implemented in our numerical model consists in successively solving inside a time step loop the heat transfer problem, the incompressible fluid flow problem, and finally the mesh update problem (cf. figure 2).

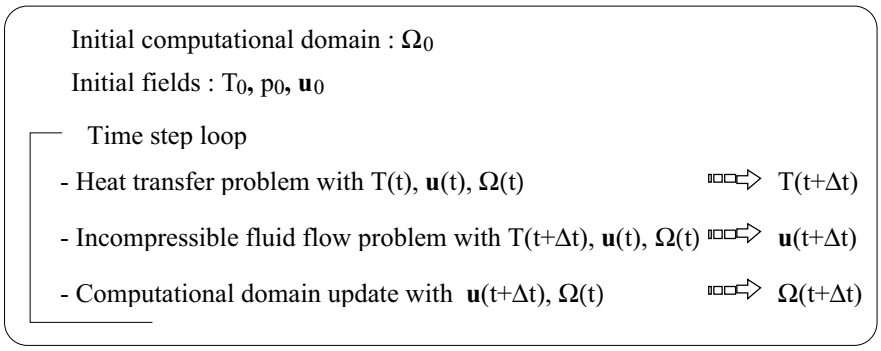

Figure 2. *The implemented segregated algorithm*

The computational mesh update is undertaken in our model by solving a steady pseudo elastic problem for the computational mesh at each time step. It is formulated in nodal mesh displacement variables in order to explicitly satisfy a kinematic boundary condition all over the fluid flow domain boundary which states a vanishing normal component of the relative velocity between the liquid fluid flow and the mesh (Rabier *et al*., 2003).

3.2. *Finite element formulations*

The three separate finite element (weak) formulations and their respective algebraic systems are obtained following the standard approach used in the finite element method (Dhatt *et al*., 1981), (Carey *et al*., 1986), (Hughes, 1987): **d** and **w** are the nodal mesh displacement and velocity in the ALE framework, respectively. δT, δ**u**, δp and δ**d** are the weighting functions associated with the unknown fields T, **u**, p and **d**, respectively. Finally, H is the generalized Hooke's law matrix coefficients.

$$\int_{\Omega}\left(\rho_t Cp_i\,\delta T\left(\frac{\partial T}{\partial t}+\left(\left(\mathbf{u}-\mathbf{w}\right).\nabla\right)T\right)+k_i\left(\nabla.\delta T\right).\left(\nabla.T\right)-\delta T\,S^T\right)d\Omega$$

$$-\int_{\partial\Omega_{bs}} q_{bs}\,ds+\int_{\partial\Omega_{lv}} q_{lv}\,ds+\int_{\partial\Omega_{rc}} q_{rc}\,ds=0 \qquad [17]$$

$$\int_{\Omega}\left(\rho_l\delta\mathbf{u}\left[\frac{\partial\mathbf{u}}{\partial t}+\left(\left(\mathbf{u}-\mathbf{w}\right).\nabla\right)\mathbf{u}\right]+\mu\left[\left(\nabla\otimes\delta\mathbf{u}\right)+\left(\nabla\otimes\delta\mathbf{u}\right)^T\right].\left[\left(\nabla\otimes\mathbf{u}\right)+\left(\nabla\otimes\mathbf{u}\right)^T\right]\right)d\Omega$$

$$+\int_{\Omega}\left(p\nabla.\delta\mathbf{u}+\delta p\left(\nabla.\mathbf{u}-\frac{p}{\lambda}\right)-\delta\mathbf{u}.\left(\mathbf{f}^{\mathbf{v}}+\mathbf{S}^{\mathbf{u}}\right)\right)d\Omega+\int_{\partial\Omega_{lg}}\delta\mathbf{u}.\left(\mathbf{T}_g+\frac{\gamma}{R}\mathbf{n}+\frac{\partial\gamma}{\partial s}\mathbf{t}_g\right)ds=0$$

[18]

$$\int_{\Omega}\left(\left[\left(\nabla\otimes\delta\mathbf{d}\right)+\left(\nabla\otimes\delta\mathbf{d}\right)^T\right].\overline{\overline{\mathbf{H}}}.\left[\left(\nabla\otimes\mathbf{d}\right)+\left(\nabla\otimes\mathbf{d}\right)^T\right]\right)d\Omega=0 \qquad [19]$$

The weak integral form associated with the heat transfer problem [17] is discretized in space with Lagrange iso-parametric finite elements, using tri-quadratic approximations in each element of C^0 continuity. These approximations led us to use 27 node hexahedral (brick) elements for domain integrals and 9 node quadrilateral elements for boundary integrals.

Concerning the incompressible fluid flow problem [18], we have used the same finite element approximations for the velocity components as the temperature. Nevertheless dealing with the pressure variable, one has to pay much attention in order to have its algebraic system efficiently solved owing to the incompressibility constraint. Consequently, we have used a penalized formulation, which introduce a numerical link between the pressure and the incompressibility constraint. Besides, provided one chooses a discontinuous pressure approximation between elements (non-nodal approximation for the pressure), it allows us to eliminate the pressure variable at the element level (static condensation). Therefore the resulting algebraic system for the fluid flow problem has a reduced dimension (it only contains the velocity degrees of freedom), but on the bad side this turns out to come with a very poor condition number, which is a heavy drawback to efficiently solve it.

Finally the weak integral form associated with the pseudo elastic problem [19], which enables us to update the moving boundary computational domain is also

performed with the same approximations as the temperature and velocity components.

On the other hand the temporal scheme used is the first order backward Euler for both the heat transfer and fluid flow problems, whereas a steady solution of the pseudo elastic problem is performed at each time step.

3.3. *Solution strategy*

The computations involved in the thermo-hydraulic simulation of high energy welding processes are well known to be highly time-consuming for several reasons. First of all, as the whole process is to be simulated, only transient computations could be relevant. Furthermore, a three dimensional model is required to reproduce the keyhole dynamics owing to the welding speed (scan speed). Finally, the mathematical models related to the welding process physics are highly non-linear. So all these reasons led us to develop a research code specifically designed to run high performance computers, taking advantage of parallel processing. It has been written on top of the Petsc library (Balay *et al*., 1997), (Balay *et al*., 2003), in order to reach the difficult trade off between performance and ease to develop.

The algebraic systems associated with the heat transfer and fluid flow problems are non-linear. The former is highly non-linear owing to the latent heat release or absorption involved in the solid-liquid and liquid-vapor phase change on the one hand, and on the other hand to the radiative heat exchange considered in the boundary conditions. The incompressible fluid flow problem is not only non-linear owing to the usual avdective term, but also due to the modified source term which accounts for the fluid flow in the mushy zone. Consequently their associated algebraic systems are iteratively solved with a Newton-Raphson procedure up to a user-defined convergence criterion for the residual.

As already mentioned the chosen segregated algorithm allows us to select separately the most efficient solution algorithm for each discrete sub-problem. Therefore, the algebraic systems associated with the heat transfer and the steady pseudo elastic problems, which have a sufficiently acceptable condition number can be efficiently solved with parallel iterative procedures available in Petsc. Our experience drawn from various comparative tests indicated us to select the combination of a Krylov based method (Bi-conjugate gradient stabilized method, BCGS) preconditioned with bloc diagonal Jacobi algorithm (Bjacobi), which gives us satisfactory parallel efficiency in most of the considered computations. Conversely the algebraic system associated with the incompressible fluid flow problem is so very poorly conditioned (for the considered penalty coefficient, $\lambda=10^8$) that no preconditioned iterative solver available in Petsc is able to efficiently solve it in parallel. Consequently we have chosen to use the Spooles solver (Ashcraft et al., 1999), a parallel direct solver, which can be easily interfaced with Petsc.

4. Applications

The finite element models used to build up the present high energy welding model have been separately validated and used in several previously published works (Medale et al., 2000), (Medale et al., 2002), (Rabier et al., 2003). So in this paper we are mainly concerned to numerically study the influence of various physical phenomena on the whole heat transfer related to high energy welding processes. At first we consider a simplifying conductive regime (in which the liquid-gas interface could be assumed flat) to study the influence on the melted pool geometry of several difficult to experimentally estimate contributions. Next, we consider the coupled heat transfer and fluid flow problem in a steady capillary regime for which a keyhole of imposed cylindrical shape is set up in the computational domain. Finally, we present a study case where all the dynamics (keyhole, fluid flow and heat transfer) is consistently computed within our numerical model. In the following application examples, we have always considered the same work-piece material properties (which corresponds to a stainless steel alloy):

$\rho = 6500\ kg.m^{-3}$; $\mu = 0.003\ N.s.m^{-2}$; $\gamma_0 = 0{,}1\ N.m^{-1}$; $d\gamma/dT = -0.0003\ N.m^{-1}.K^{-1}$;
$C_P = 1000\ J.kg^{-1}.K^{-1}$; $k_{liq} = 100\ W.m^{-1}.K^{-1}$; $k_{sol} = 200\ W.m^{-1}.K^{-1}$; $T_{sol} = 1600\ °C$;
$T_{liq} = 1650\ °C$; $\varepsilon = 0.5$; $h = 10\ W.m^{-2}.K^{-1}$; $\Delta H = 250\ KJ/kg$.

All the computations have been performed in three space dimensions, but assuming a longitudinal symmetry plane to exist as sketched in figure 3.

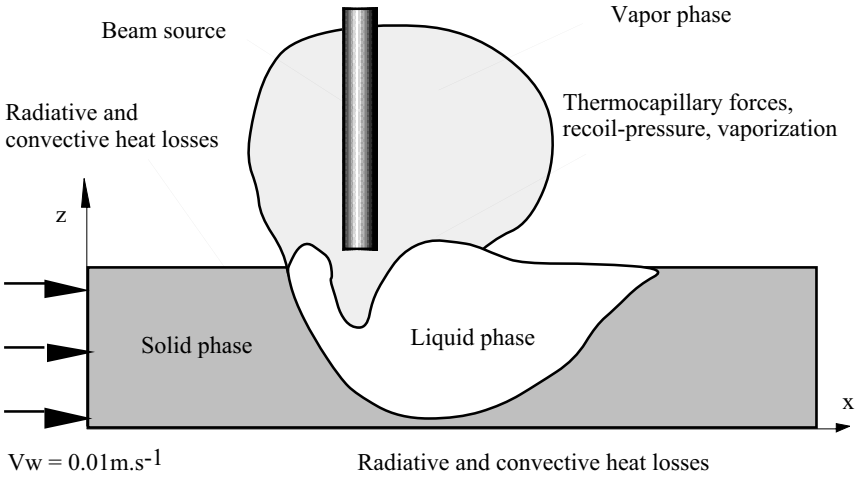

Figure 3. *Sketch of the welding configuration in the longitudinal symmetry plane*

Furthermore, all the computations are performed in a reference frame associated with the beam source, involving thus the work-piece enters the computational domain with the inlet velocity (V_w = 0.01 ms^{-1} in the considered examples).

4.1. *Conductive regime: no keyhole (flat free surface)*

In this section we deal with a rather simplifying geometrical configuration for which the free surface deformation could be assumed as negligible (welding conductive regime). Keeping in mind this assumption, we have performed a parametric study to determine the influence of some physical phenomena on observable welding characteristics (melted pool size and shape). Namely, we have examined the influence of the radiative and convective heat exchanges over the computational domain boundaries, the solid-liquid phase change latent heat release/absorption, and finally advective fluid flow contribution in the melted pool.

The computational domain is a parallelepiped (l = 80 mm, w = 40 mm, h = 2 mm), which only extends on one side of the longitudinal symmetry plane (the y = 0 plane). The computational mesh is made up of 50 000 H27 finite elements (100x50x10), built up on 42 6321 nodes. The maximum value of the applied heat source flux (cf. [1]) is in this example $I_0=2.10^8$ Wm^{-2}, and the beam radius is r_b = 1 mm.

The influence of the considered physical phenomena on the melted pool (defined to be the computational zone for which the local temperature is greater than the solidus temperature) is reported in table 1. The length and width of the melted pool is compared for the following configurations. The reference computation (C1) is defined to be the most complete one (all physical mechanisms described in section 2). All the following configurations are based on the reference computation, except one contribution, which is not considered. In the second configuration (C2), the radiative and convective heat exchange are not considered. In the third configuration (C3), the solid-liquid latent heat enthalpy is not taken into account in the model. Finally, in the fourth configuration (C4), no natural convection fluid flow is considered in the melted pool (its velocity remains the welding velocity).

Configurations	C1	C2	C3	C4
Melted pool length (L in mm)	13.6	15.1	10.9	7.7
Relative variation of L (%)		+11	-20	-43
Melted pool width (W in mm)	7	7.6	7.1	5.85
Relative variation of W (%)		+9	+1.5	-16

Table 1. *Quantitative influence on the melted pool sizes (length and width) for several physical modeling*

As expected (see table 1), the fluid flow contribution to heat transfer in the melted pool (advective heat transfer component) plays a significant part on the melted pool size. Indeed, if one compares configuration C4 with respect to the full computation (C1), it appears a 43% and a 16% decrease on the melted pool length and width, respectively. This means that the thermocapillary driven convection not only enhances heat transfer within the work-piece, but also lowers the high temperature area close to the beam source impact zone (see figure 4).

On the other hand, dropping out the solid-liquid phase change enthalpy from the computation results in a contrasted behavior: a significant length decrease (-20%) associated with a very slight width increase (+1.5%). The interpretation of this results is here again strongly related to the advective heat transfer in the melted pool. Indeed, a huge temperature gradient appears on the upper surface just in front of the beam source owing to the welding velocity.

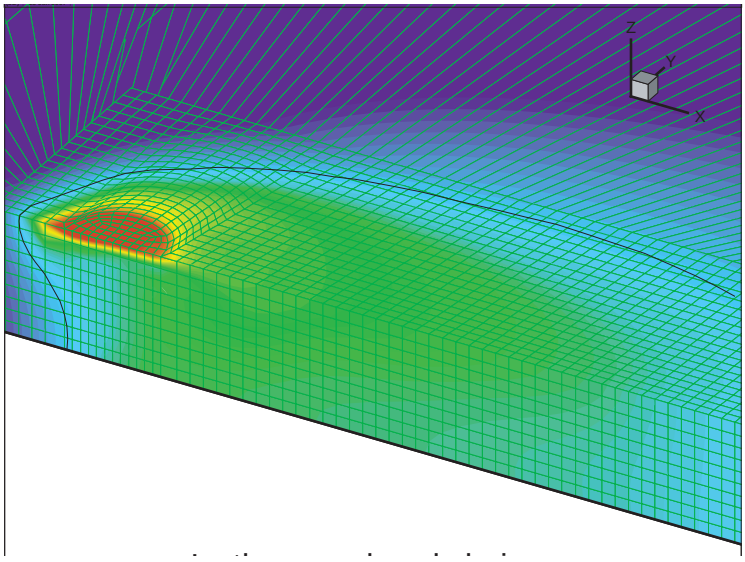

Figure 4. *Conductive regime: computational mesh and temperature field in the longitudinal symmetry plane and upper free surface*

It induces an intense surface tension driven convection which develops in the form of a horseshoe roll (see figure 5). So the solid-liquid phase change enthalpy is absorbed during melting in this region (of quite small volume), whereas it is later on released downstream into a solidifying zone of much higher volume and much smaller temperature gradient. This explains the highest influence of the solid-liquid

phase change enthalpy on the longitudinal direction (the welding direction) compared to the transversal one. This influence is mainly located at the downstream melted pool tail, where the latent enthalpy release changes notably the solid-liquid interface location (owing to the small temperature gradient in this zone). In the considered welding case of quite small thickness work-piece, it is also noteworthy to discuss the fluid flow structure in the melted pool. Indeed, as the melting temperature is also exceeded in the whole work-piece thickness, thermocapillary forces act on both the upper and lower free surface. They induce thus a counter-rotating roll of low intensity in the downstream lower corner (see figure 5).

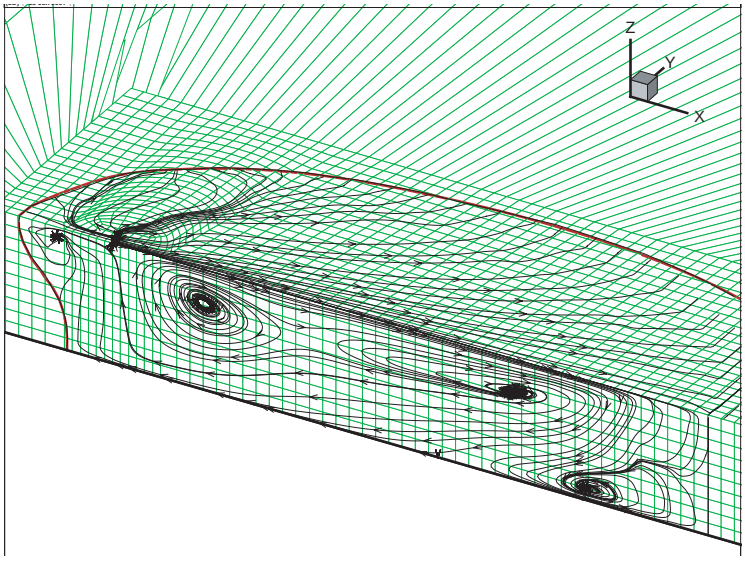

Figure 5. *Conductive regime: computational mesh and streamlines in the longitudinal symmetry plane and upper free surface*

Finally, although a quite crude radiative and convective heat exchange model has been considered in the present computations [8], it provides a non-negligible influence on the global heat transfer owing to the high temperature levels involved. Besides, it produces a quite comparable influence on the melted pool size on both directions (roughly +10% on the melted pool length and width when it is dropped).

4.2. *Capillary regime: keyhole of imposed cylindrical shape*

Let us now move on to the characteristic configuration of high energy density welding for which a deep capillary hole forms owing to intense recoil pressure: the keyhole configuration. As a first modeling stage, we have set up in the

computational domain a capillary hole of an imposed cylindrical shape (see figure 6 left). The computational domain represents the first 2 mm from the upper surface of work-piece, and the capillary hole diameter is set to 0.4 mm. The spatial scale is non-dimensionalized with respect of the computational domain thickness, and it extends only on one side of the vertical longitudinal (with respect to the welding velocity) plane going through the beam source axis, since longitudinal symmetry is here again assumed. The mesh is made up of 36 000 H27 finite elements, built on 30 2621 nodes (see figure 6 right).

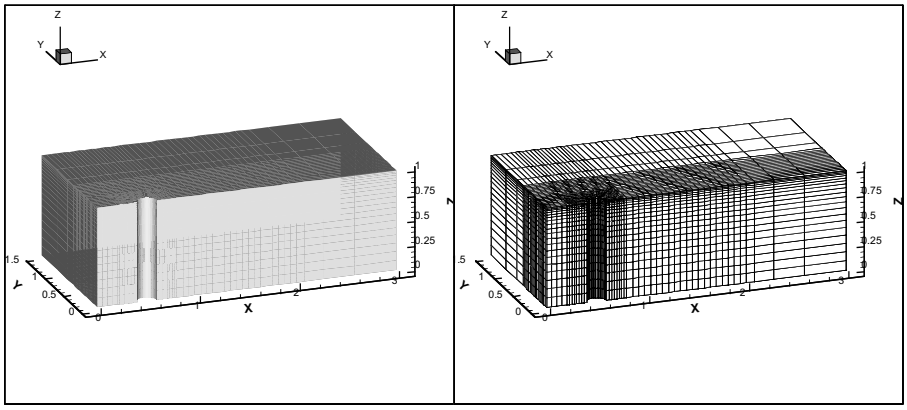

Figure 6. *Keyhole of imposed cylindrical shape: computational domain (left) and mesh (right)*

Here again the geometry is imposed to its initial shape throughout the whole computation, however the beam source energy is now delivered all over the capillary-hole wall, where a constant temperature (the metal vaporization temperature, $T_v = 3080°C$) is imposed in our modeling. Therefore the thermal penetration in the vertical direction is much highly enhanced (see figure 7), as observed in the capillary welding regime. The isotherms are mainly distorted in the first upper half of the domain behind the capillary hole. One can notice in figure 8 this region corresponds to the most intense natural convection fluid flow, mainly driven by surface tension gradients. Therefore the fluid flow in the melted pool is structured in a flat roll below the free surface, and it extends in the vertical direction with weaker and weaker magnitude. Furthermore in this configuration the liquid fluid flow arriving in front of the capillary hole is obliged to twist around the cylindrical obstacle, which produces a larger melted pool size in the transversal direction, compared to the case without capillary hole.

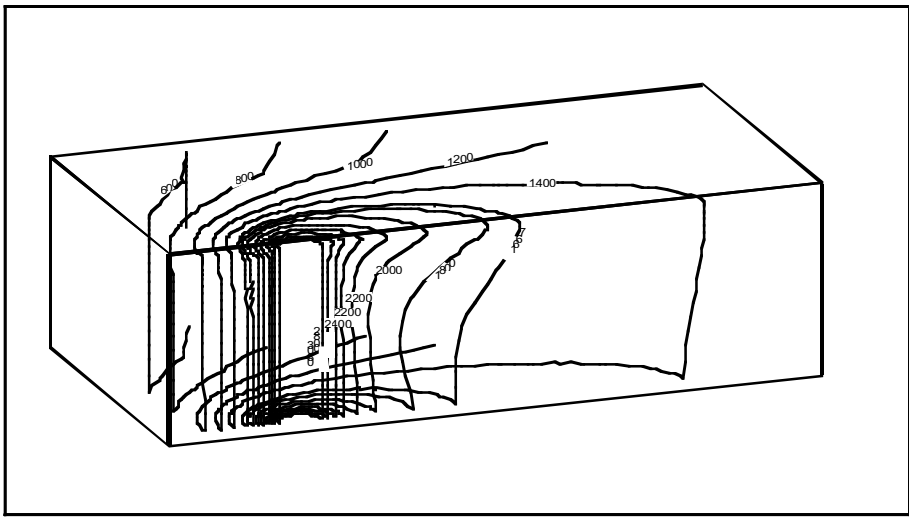

Figure 7. *Keyhole of imposed cylindrical shape: temperature field in the longitudinal symmetry plane and on the upper free surface*

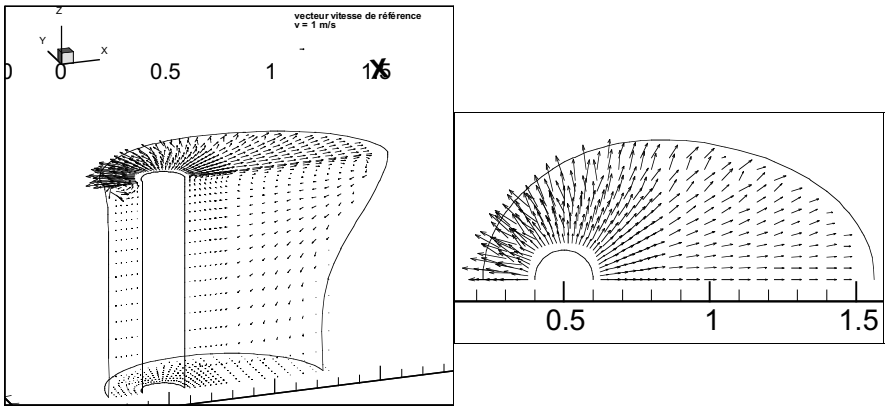

Figure 8. *Keyhole of imposed cylindrical shape: velocity field in the longitudinal symmetry plane and on the upper free surface (left), top view of the velocity field over the free surface (right)*

4.3. *Consistently computed keyhole*

Finally, we have considered the case where the keyhole is consistently computed during the computation. The initial computational domain is a parallelepiped, non-dimensionalized with respect of the height of the work-piece, of extension (l/h = 3, w/h = 1.5, h = 2 mm). Its associated mesh is made up of 4500 H27 finite elements, built on 39 711 nodes.

The present computation features a constant recoil pressure ($Tg / \rho Vw^2 = 20$), whereas all the other input been the same as in §4.1. The considered ratio, which represents the strength of the vapor pressure with respect to the kinetic energy (based on the welding velocity), is quite typical of actual laser beam welding in capillary regime (deep keyhole). In an early stage of the computation, a conductive like regime is encountered (see figure 9). However the thermal field associated with this ephemeral conductive regime is by far different from the one observed in §4.1, because in the present case the melted pool is of very narrow extension and the associated fluid flow is of very small magnitude.

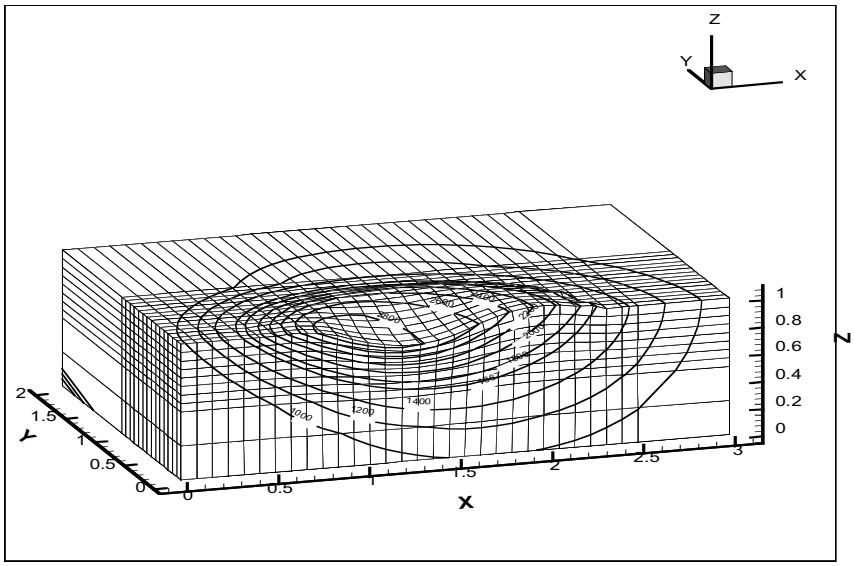

Figure 9. *Temperature field in the longitudinal symmetry plane and the upper free surface for the consistently computed keyhole for an early drilling stage*

In a later instant the drilling mechanism becomes the leading phenomena in the vicinity of the applied source intensity. The velocity field (see figure 10) displays a piston-like effect in the melted pool, the liquid metal flows downward in the applied energy region and flees on the sides. The liquid metal arriving in front of the beam

source can in this configuration twist around on the sides or dive down to go below the expanding keyhole.

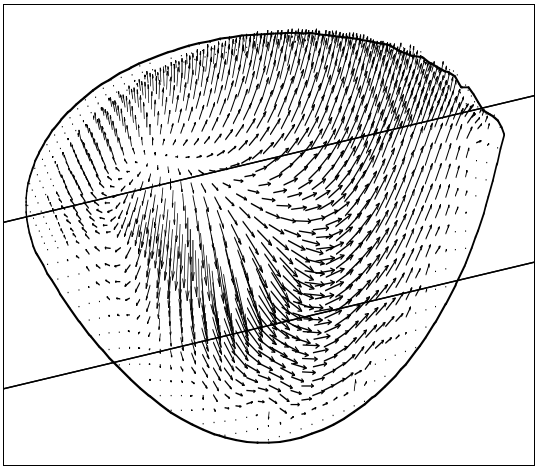

Figure 10. *Velocity field in the longitudinal symmetry plane and the upper free surface for the consistently computed keyhole during the drilling stage*

5. Conclusions

In this paper a finite element model has been proposed to compute the heat transfer in the whole work-piece submitted to high energy welding processes. This model takes into account the dispersed phases (ambient gas, shield gas, metallic vapors) in a rather simplified way, whereas the condensed phases (solid, mushy and liquid metal) is considered in a more comprehensive way. The liquid-gas interface, and the whole keyhole dynamics are tracked thanks to a free surface fluid flow model, and the solid-liquid interface is implicitly accessed thanks to an enthalpy formulation of the energy conservation equation.

Several three dimensional application examples have been considered, featuring various levels of deposited energy density and their associated computational complexity. At the lowest level, a moderate energy density is applied at the upper free surface, and the local deformation is negligible, as could be reasonably assumed in welding conductive regimes. Thanks to a cheaper numerical handling of this particular configuration, we have thus conducted a numerical parametric study. It turns out from that study the global heat transfer in the work-piece is predominantly driven by advection in the melted pool. It produces a strong mixing in the liquid metal, which results in a high temperature averaging process. Furthermore, the solid-liquid phase change latent heat plays also an important part in the size of the melted

pool, and the related thermal field. On the one hand, it strengthens the temperature gradients at the upstream forefront of the melted pool, and conversely it smoothes them at the downstream tailing edge where solidification takes place.

At a higher density of applied energy, a keyhole forms and can no longer be ignored in any modeling owing to its significant role in the whole welding process. Therefore we have dealt with it in two different ways: in the simplest one, we have imposed a capillary hole of fixed cylindrical shape in the computational model; while in a more realistic computation we have consistently computed its early expansion stages.

6. References

Anisimov S.I., « Vaporization of metal absorbing laser radiation », *Sov. Phys. JETP 27*, 1968, p. 182-183.

Ashcraft C., Grimes R., « SPOOLES: An Object-Oriented Sparse Matrix Library », *Proceedings of the 1999 SIAM Conference on Parallel Processing for Scientific Computing*, San Antonio, Texas, USA, March 22-27, 1999.

Balay S., Gropp W.D., Mc Innes L.C., Smith B.F., « Efficient Management of parallelism in object oriented numerical software librairies », *Modern Software Tools in Scientific Computing*, Arge E. and Bruaset A.M. and Langtangen H.P. (Ed.), Birkhauser Press, 1997, p. 163-202.

Balay S., Buschelman K., Gropp W.D., Kauskik D., Mc Innes L.C, Smith B.F., Petsc home page, 2003, (http://www.mcs.anl.gov/petsc).

Belytschko T., Liu W.K., Moran B., *Nonlinear finite elements for continua and structures*, New York, J. Wiley & Sons Ltd., 2000.

Bennon W.D., Incropera F.P., « A continuum model for momentum, heat and species transport in binary solid-liquid phase change systems - 1. Model formulation, 2. Application to solidification in a rectangular cavity », *Int. J. Heat Mass Transf.*, Vol. 30, n° 10, 1987, p. 2161-2187.

Carey G.F., Oden J.T., *The Texas Finite Element Series*, Prentice-Hall, Englewood Cliffs, New Jersey, 1986.

Crank J., *Free and moving boundary problems*, Oxford, Oxford University Press, 1984.

Dhatt G., Touzot G., *Une présentation de la méthode des éléments fins*, Paris, Maloine Ed., 1981.

Duley W.W., *Laser Welding*, United States, Wiley Interscience, 1999.

Fabbro R., Chouf K., « Keyhole modeling during laser welding », *J. Phys. D: Appl. Phys.*, vol. 87, 2000, p. 4075-4083.

Ganesh R.K., Faghri A., Hahn Y., « A generalized thermal modelling for laser drilling process – I. Mathematical modelling and numerical methodology », *J. Heat Mass Transfer*, vol. 40, 1997, p. 3351-3360.

Ganesh R.K., Faghri A., Hahn Y., « A generalized thermal modelling for laser drilling process – II. Numerical simulation and results », *J. Heat Mass Transfer*, vol. 40, 1997, p. 3361-3373.

He X., Fuerschbach P.W., DebRoy T., « Heat transfer and fluid flow during spot welding of 304 stainless steel », *J. Phys. D: Appl. Phys.*, vol. 36, 2003, p. 1388-1398.

Hirt C.W., Amsden A.A., Cook J.L., « An arbitrary Lagrangian-Eulerian computing method for all flow speeds », *J. Comput. Phys*., vol. 14, 1974, p. 227-253.

Ho C.Y., Wen M.Y., « Distribution of the laser intensity absorbed by the keyhole wall in laser processing », *Journal of Materials Processing Technology*, vol. 145, 2004, p. 303-310.

Hughes T.J.R., *The finite element method: linear static and dynamic finite element analysis*, Prentice-Hall, Englewood Cliffs, New Jersey, 1987.

Hughes T.J.R., Liu W.K., Zimmermann T.K., « Lagrangian-Eulerian finite element formulation for incompressible viscous flows », *Comput. Methods Appl. Mech. Engrg*., vol. 33, 1981, p. 329-349.

Jouvard J.-M., Girard K., Perret O., « Keyhole formation and power deposition in ND : YAG laser spot welding », *J. Phys. D: Appl. Phys.,* vol. 34, 2001, p. 2894-2901.

Kaplan A., Mizutani M., Katayama S., Matsunawa A., « Unbounded keyhole collapse and bubble formation during pulsed laser interaction with liquid zinc », *J. Phys. D: Appl. Phys.,* vol. 35, 2002, p. 1218-1228.

Ki H., Mohanty P.S., Mazumder H., « Modelling of high density laser material interaction using fast Level Set method », *J. Phys. D: Appl. Phys.,* vol. 34, 2001, p. 364-372.

Knight C.J., « Theoretical modelling of rapid surface vaporization with back pressure », *AIAA J.,* vol. 17, 1979, p. 519-523.

Knight C.J., « Transient vaporization from a surface into vacuum », *AIAA J.,* vol. 20, 1982, p. 950-961.

Medale M., Cerisier P., « Numerical Simulation of Bénard-Marangoni Convection in small aspect ratio containers », *Num. Heat Transf. A*, vol. 42, 2002, p. 55-72.

Medale M., Jaeger M., Kaiss A. « Finite element analysis of the action of buoyancy induced and thermocapillary flow on the melting of tin in a 2D square cavity », *Comp. Ass. Mech. Engrg. Sci.*, vol. 7, 2000, p. 307-320.

Ni J., Incropera F.P., « Extension of the continuum model for transport phenomena occuring during metal alloy solidification - 1. The conservation equations, 2. Microscopic considerations », *Int. J. Heat Mass Transf*., vol. 38, n° 7, 1995, p. 1271-1296.

Rabier S., Medale M., « Computation of free surface flows with a projection FEM in a moving mesh framework », *Comput. Methods Appl. Mech. Engrg*., vol. 192, 2003, p. 4703-4721.

Rappaz M., « Modelling of microstructure formation in solidification processes », *Int. Mater. Rev*., Vol. 34, 1989, p. 93-123.

Reddy M.P., Reddy J.N., « Numerical simulation of forming processes using a coupled fluid flow and heat transfer model », *Int. J. Num. Meth. Eng*, Vol. 35, 1992, p. 807-833.

Semak W., Bragg W.D., Damkroger B., Kempkas S., « Temporal evolution of the tempertaure field in the beam interaction zone during laser material processing », *J. Phys. D: Appl. Phys.*, vol. 32, 1999, p. 1819-1825.

Semak W., Matsunawa A., « The role of recoil pressure in energy balance during laser – materials processing », *J. Phys. D: Appl. Phys.,* vol. 30, 1997, p. 2541-2552.

Shyy W., Udaykumar H.S., Rao M.M., Smith R.W., *Computational fluid dynamics with moving boundaries*, Washington D.C., Hemisphere, 1996.

Solana P., Kapadia P., Dowden J.M., Marsden P.J., « An analytical model for laser drilling of metals with absorption within the vapour », *J. Phys. D: Appl. Phys*., vol. 32, 1999, p. 942-952.

Solana P., Negro G., « A study of the effect of multiple reflections on the shape of the keyhole in the laser processing of materials », *J. Phys. D: Appl. Phys.*, vol. 30, 1997, p. 3216-3222.

Sudnik W., Radaj D., Breitschwerdt S., Erofeew W., « Numerical simulation of weld pool geometry in laser beam welding », *J. Phys. D: Appl. Phys*., vol. 33, 2000, p. 662-671.

Voller V.R., Prakash C., « A fixed grid numerical modelling methodology for convection-diffusion mushy region phase change problems », *Int. J. Heat Mass Transf*., vol. 24, 1987, p. 1709-1718.

Voller V.R., Swaminathan C.R., Thomas B.G., « Fixed grid techniques for phase change problems: a review », *Int. J. Num. Meth. Eng*., vol. 30, 1990, p. 875-898.

Ytrehus T., Bergstrom T., « Theory and experiments on gas kinetics in evaporation in rarefied gas dynamics », AIAA J., New York, edited by J.L Potter , 1977, p. 1197-1212.